Switching stabilizing controller design for an inverted pendulum system platform

Jonathan Chandra[1,2], Tua Agustinus Tamba[2], Ali Sadiyoko[2]
[1]Department of Mechanical Engineering, Faculty of Science and Engineering, University of Groningen, Groningen, Netherlands
[2]Department of Electrical Engineering, Faculty of Industrial Technology, Parahyangan Catholic University, Bandung, Indonesia

ABSTRACT

This paper reports the development and switching controller design of an inverted pendulum system (IPS) platform. The euler-lagrange approach is first used to model the dynamics of the IPS which takes into account the impact of friction forces during its movements. The paper then derives a switching control method to swing the pendulum rod into the neighborhood of and stabilizing it at the equilibrium point. The implemented switching controller consists of: i) a nonlinear swing up control which brings the pendulum to the vertical position and ii) a linear stabilizing control which maintains the pendulum rod to remain in a vertical position around the neighborhood of the vertical axis. The nonlinear controller is constructed using lyapunov's method while the linear controller is designed using linear quadratic regulator (LQR) method framework. Simulation and experimental results are presented to show the effectiveness of the proposed switching controller.

Corresponding Author:

Tua Agustinus Tamba
Department of Electrical Engineering, Faculty of Industrial Technology, Parahyangan Catholic University
Jl. Ciumbuleuit no. 94, Bandung 40141, Indonesia
Email: ttamba@unpar.ac.id

1. INTRODUCTION

One prominent benchmark for evaluating control systems' analysis and design framework is the inverted pendulum system (IPS) [1]–[4]. An IPS platform typically composed by a horizontally moving cart and a pendulum rod that is mounted on the cart's top [5]. The objective of the IPS control is thus to regulate the cart's movement so that the rod can be rotated and then maintained in a vertical upward position (Figure 1) [6]. Such a control objective has in fact been known to be the working principle of several practical technological applications which includes controller design for differential drive mobile robots with a self balancing feature, rocket launcher with vertical take-off and landing capability [7]–[9].

Various results have been reported in literature on topics related to the analysis and control system design of IPS. For instance, linear quadratic regulator (LQR) and proportional-integral-derivative (PID) control are used in [10], [11], respectively, to stabilize IPS prototypes' linearized models. The works in [12] [13], on the other hand, used fuzzy logic controllers (FLC) to swing up and stabilize an IPS prototype using its linearized model. However, the performance of FLC-based controllers is known to be very dependent on the designer's heuristics when defining the logic of the control rules. The works in [14]–[17] proposed energy-based methods within Lyapunov's stability framework for control system design of IPS platform. The implementations of such energy-based control design methods are typically formulated as optimization problems which often results

in high computational demands/loads. Moreover, the obtained controller gains which guarantee lyapunov's stability of the closed system are often capable of only guaranteeing the pendulum rod to oscillate within a small neighborhood of the IPS's unstable equilibrium which is defined by as the vertical upward position. In particular, real-time implementation of the used energy-based control methods are not yet examined or extensively reported in some of these literature.
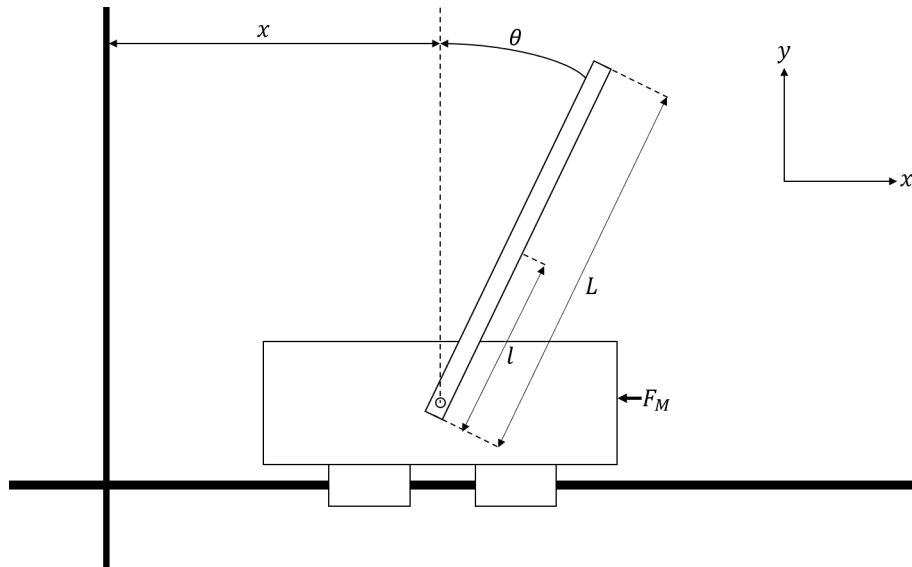

Figure 1. Sketch of an IPS on a cart

This paper further continues our initial simulation study in [18], [19] and reports the design and real-time implementation of energy-based methods for simultaneous dynamic model development and stabilizing controller design of an IPS prototype. This paper uses euler-lagrange method to derive an experimentally-tested model for a developed IPS prototype which incorporates the friction force effect that is induced by the IPS' cart movement. A switching stabilizing control law that can swings the pendulum rod up to reach the neighborhood of and then stabilizes it at the desired unstable equilibrium point is then designed. Results from simulation and experimental evaluations are reported to illustrate the proposed stabilizing control scheme's effectiveness.

2. SYSTEM DESCRIPTION AND MODELING
2.1. IPS configuration

Figure 2 sketches the considered IPS. It consists of two main parts, namely i) a cart of mass M that is moving horizontally on a rail of finite length along the x axis and ii) a pendulum rod with length $2l$ and mass m with one end attached on the cart to allow the other end moves in a circular motion. In Figure 1 is the angle from the pendulum rod to the vertical y axis at time t, $x(t)$ denotes the horizontal position of the cart along the rail at time t, and l denotes the half length of the pendulum rod which is measured as the distance from the pivot point of the rod to its center of mass. F_M denotes the horizontal input force that acts on the cart.

Figure 2 depicts the hardware configuration of the considered IPS both from the side (Figure 2(a) and top Figure 2(b) views. It can be seen in these figures that the IPS is composed by two major components, namely the electric circuit and mechanical system. The electric circuit part is used to handle data acquisition system and commands for actuator movements based on the developed control law. The mechanical system part is assembled from two main components, namely a pendulum rod and a cart which carries the rod.

The input and output data for controller design purposes are handled using an Arduino due microcontroller. Two rotary encoders are also connected to microcontroller to obtain the IPS' cart position and the pendulum rod's deviation angle measurements. To regulate the cart's position/movement on the rail, a timing belt was attached to the IPS' cart to transform the rotation of a connected DC motor into the cart's horizontal movement. A personal computer (PC) is used to manage, reserve and display the input/output data of the IPS.
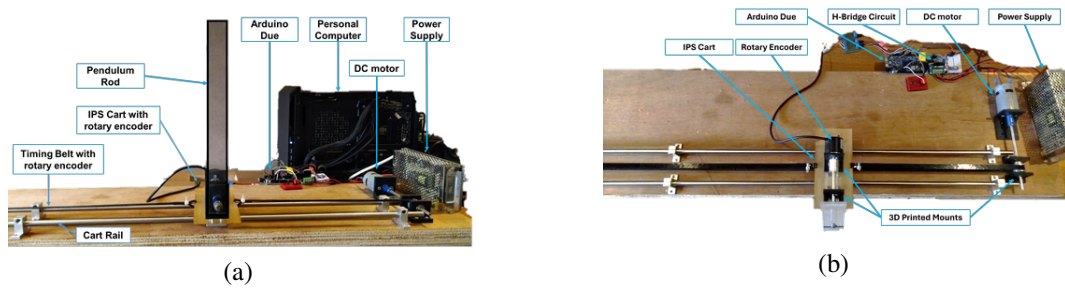
Figure 2. Hardware components of the IPS from: (a) front and (b) top views

2.2. Mathematical model

Figure 3 shows the free body diagram (FBD) of the considered IPS which consists of the FBD of a moving cart along the horizontal x axis shown in Figure 3(a) and the FBD of the attached pendulum rod which rotates with respect to the vertical y axis as shown in Figure 3(b). The IPS model is derived using euler-lagrange (EL) method based on its lagrangian function, $\mathcal{L}$, which captures the difference between the IPS's kinetic (E_K) and potential (E_P) energies. In particular, E_K is induced by both the cart and pendulum rod motions, whereas E_P is defined solely by the pendulum rod's position.
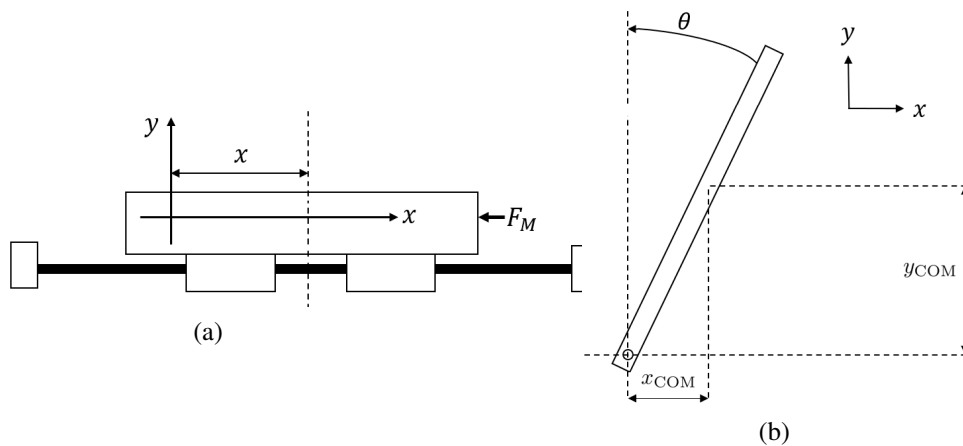

Figure 3. Free body diagrams of: (a) IPS cart and (b) pendulum rod

Let $\dot{x}(t) = dx(t)/dt$. By Figure 3, the kinetic energy E_K^c of the cart is defined as: $E_K^c = \frac{1}{2}M\left(\dot{x}(t)\right)^2$. The projections of the rod's center of mass (COM) position and velocity on the horizontal axis are $x_{\text{COM}}(t) = x(t) + l\sin(\theta(t))$ and $\dot{x}_{\text{COM}}(t) = \dot{x}(t) + l\dot{\theta}(t)\cos(\theta(t))$, while on the vertical axis are given by $y_{\text{COM}}(t) = l\cos(\theta(t))$ and $\dot{y}_{\text{COM}}(t) = -l\dot{\theta}(t)\sin(\theta(t))$. The pendulum rod's kinetic energy E_K^p takes the form.

$$E_K^p = (m/2)\left[(\dot{x}_{COM}(t))^2 + (\dot{y}_{COM}(t))^2\right] \tag{1}$$

Thus, the total kinetic energy of the IPS becomes $E_K = E_K^c + E_K^p$, and its total potential energy is defined as $E_P = E_P^p = lmg\left(\cos(\theta(t)) - 1\right)$. The lagrangian $\mathcal{L} := E_K - E_P$ of the IPS may then be defined as in (2).

$$\mathcal{L} = \frac{1}{2}M\left(\dot{x}(t)\right)^2 + lm\dot{\theta}(t)\dot{x}(t)\cos\left(\theta(t)\right) + \frac{1}{2}m(\dot{x}(t))^2 + \frac{1}{2}l^2m(\dot{\theta}(t))^2 + lmg\left(1 - \cos\theta(t)\right) \tag{2}$$

given the system lagrangian in (2), the IPS model can be derived using EL in (3):

$$\frac{d}{dt}\left(\frac{\partial\mathcal{L}}{\partial\dot{x}}\right) - \frac{\partial\mathcal{L}}{\partial x} = F_1 \qquad\qquad \frac{d}{dt}\left(\frac{\partial\mathcal{L}}{\partial\dot{\theta}}\right) - \frac{\partial\mathcal{L}}{\partial\theta} = F_2 \tag{3}$$

where $F_1=F_M$, while $F_2=\gamma_r\dot{x}(t)$ denotes the friction force with coefficient γ_r that is induced by the swinging of the pendulum rod at the pivoting point. Using (2) on (3), the IPS model can be rewritten in (4a) and (4b).

$$(m + M)\ddot{x}(t) + lm\cos(\theta(t))\ddot{\theta}(t) - lm\sin(\theta(t))(\dot{\theta}(t))^2 = F_M, \tag{4a}$$

$$lm\cos(\theta(t))\ddot{x}(t) + l^2m\ddot{\theta}(t) - lmg\sin(\theta(t)) = \gamma_r\dot{\theta}(t). \tag{4b}$$

let $q(t) := [q_1(t), q_2(t)]^T = [x(t), \theta(t)]^T$ be the generalized variable. Then (4) can be rearranged into (5).

$$M\left(q(t)\right)\ddot{q}(t) + C\left(q(t), \dot{q}(t)\right)\dot{q}(t) + G(q(t)) + D(\dot{q}(t)) = u(t), \tag{5}$$

with vector and matrix elements as in (6).

$$q(t) = \begin{bmatrix} x(t) \\ \theta(t) \end{bmatrix} \quad M(\cdot) = \begin{bmatrix} (m + M) & lm\cos(\theta(t)) \\ lm\cos(\theta(t)) & l^2m \end{bmatrix} \quad C(\cdot) = \begin{bmatrix} 0 & -lm\dot{\theta}(t)\sin(\theta(t)) \\ 0 & 0 \end{bmatrix}$$
$$D(\cdot) = \begin{bmatrix} 0 & 0 \\ 0 & \gamma_r \end{bmatrix} \quad G(\cdot) = \begin{bmatrix} 0 \\ -lmg\sin(\theta(t)) \end{bmatrix} \quad u(\cdot) = \begin{bmatrix} F_M \\ 0 \end{bmatrix} \tag{6}$$

note that (6) may also be written as an affine-in-control model of the form:

$$\ddot{q}(t) = f_1\left(q(t), \dot{q}(t)\right) + f_2(q(t))u(t) \tag{7}$$

where $f_1(q, \dot{q}) = (M(q)^{-1}\left[-C(q, \dot{q})\dot{q}(t) - G(q) - D(\dot{q})\right]$, $f_2(q) = -\left(M(q)\right)^{-1}D(\dot{q})$ and $u(t) = F_M$.

Introducing $x_1(t) := x(t)$, $x_2(t) := \dot{x}_1(t)$, $x_3(t) := \theta(t)$, and $x_4(t) := \dot{x}_3(t)$ as state variables, then (7) may further be written (after dropping the time variable t as a nonlinear state space model in (8).

$$\begin{bmatrix} \dot{x}_1 \\ \dot{x}_2 \\ \dot{x}_3 \\ \dot{x}_4 \end{bmatrix} = \begin{bmatrix} x_2 \\ \frac{l^2m^2\sin(x_3)(lx_4^2 - g\cos(x_3)) + lm\cos(x_3)x_4\gamma_r}{\beta} \\ x_4 \\ \frac{bl^2m^2x_4^2 + (m+M)(lmg\sin(x_3) - \gamma_rx_4)}{\beta} \end{bmatrix} + \begin{bmatrix} 0 \\ \frac{1}{\beta} \\ 0 \\ \frac{lm\cos(x_3)}{\beta} \end{bmatrix} u \tag{8}$$

where $\beta = l^2m(M + m\sin^2(x_3))$ and $b = (\sin(x_3)\cos(x_3))$, while x_1 and x_3 are measurable variables. The linearization of (8) around its equilibrium can be obtained for small deviation angles θ which implies $\sin\theta \approx \theta$ with $\cos\theta = 1$. In this regard, the linearization of (8) can be written as a linear time-invariant (LTI) system (9).

$$\begin{bmatrix} \dot{x}_1 \\ \dot{x}_2 \\ \dot{x}_3 \\ \dot{x}_4 \end{bmatrix} = \begin{bmatrix} 0 & 1 & 0 & 0 \\ 0 & 0 & \frac{-mg}{M} & \frac{\gamma_r}{lM} \\ 0 & 0 & 0 & 1 \\ 0 & 0 & \frac{(m+M)g}{lM} & \frac{-(m+M)\gamma_r}{l^2mM} \end{bmatrix} \begin{bmatrix} x_1 \\ x_2 \\ x_3 \\ x_4 \end{bmatrix} + \begin{bmatrix} 0 \\ \frac{1}{M} \\ 0 \\ \frac{-1}{lM} \end{bmatrix} u(t) \quad y(t) = \begin{bmatrix} 1 & 0 & 0 & 0 \\ 0 & 0 & 1 & 0 \end{bmatrix} \begin{bmatrix} x_1 \\ x_2 \\ x_3 \\ x_4 \end{bmatrix} \tag{9}$$

2.3. Experimental measurement and estimation of model parameters

During initial experiments, it was observed that the pendulum rod is experiencing friction force when swinging on its pivoting point. A friction estimation experiment was thus conducted in which a friction force model for F_2 is assumed to be of the form $F_2 = \gamma_r\dot{\theta}$, where γ_r is the friction coefficient that needs to be estimated experimentally. The value of γ_r is estimated by initially hold the pendulum rod to $\theta \approx 0.1728\ rad$ and then let it swings until finally rests at a position where $\theta = 3.14\ rad$ (downward pointing position) as illustrated in Figure 4. Table 1 lists the model parameters of the developed IPS platform used in experiment.

By the assumed friction model, the swinging trajectory of the pendulum rod is considered to be similar with that of a second order LTI system response which is characterized by the differential in (10).

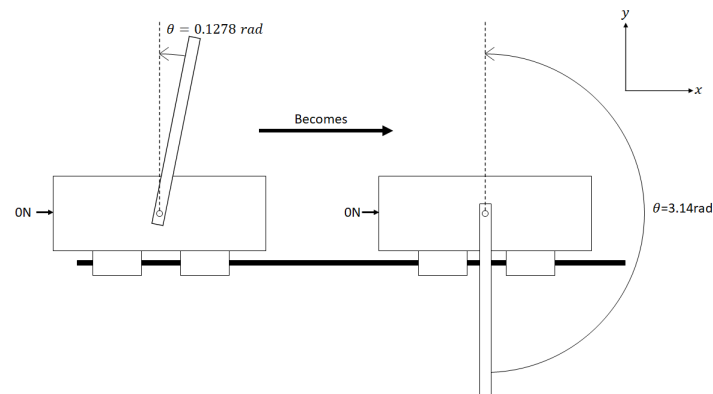$$\ddot{\theta}(t) + 2\zeta\omega_n\dot{\theta}(t) + \omega_n{}^2\theta(t) = 0 \tag{10}$$

Figure 4. Experiment illustration of the friction coefficient estimation

Table 1. IPS measured parameter

M (g)	479	479	479	479	479
m (g)	51	51	51	51	51
L (mm)	286.40	286.40	286.40	286.40	286.40

Combining (4b) with (10) and rearranging, we have that $\gamma_r/lm = 2\omega_n\zeta$ which implies $\gamma_r = 2lm\zeta\omega_n$. Figure 5 shows the pendulum rod's response which was used in (10) to obtain parameter estimates of $\omega_n = 3.0261 rad.s^{-1}$ and $\zeta = 0.026389$. In this regard, it can be determined that $\gamma_r = 0.00016872\,N.s.rad^{-1}$.
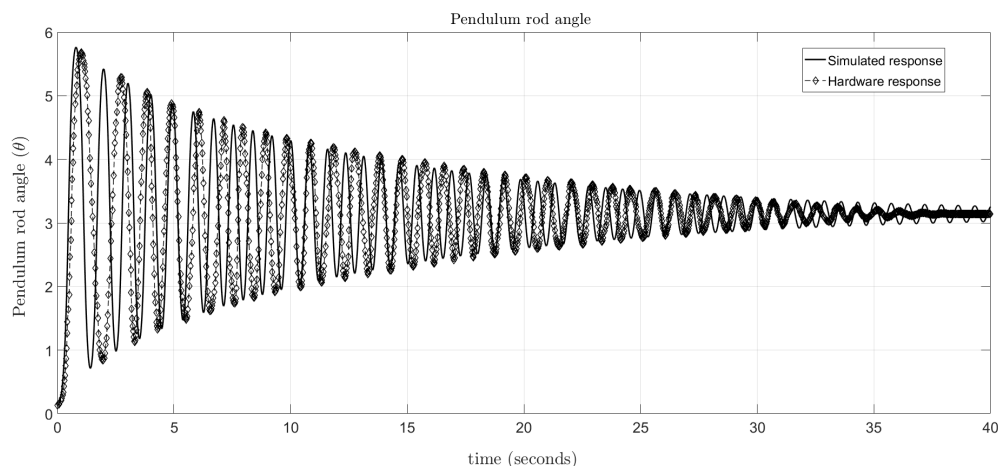

Figure 5. Pendulum rod response for friction coefficient estimation

3. RESEARCH METHODS

The main objective of IPS control is to swing up the pendulum towards the neighborhood of the upright position and then stabilize it on the vertical y axis. To achieve this objective, this research implements a switching controller which consists of: i) a nonlinear swing up controller which brings the rod to the vertical position and ii) a linear stabilizing controller which maintains the rod to remain at a vertical position around the neighborhood of the y axis [20]. The nonlinear controller is constructed using lyapunov's method on model (8), while the linear controller is designed using LQR method on model (9). The control system's block diagram is shown in Figure 6. The switching block determines which controller is activated based on IPS state. The switching occurs if the rod's orientation reach the value range of $-0.052 rad \leq \theta(t) \leq 0.052 rad$ for which an approximation of $\sin(\theta(t)) \approx \theta(t)$ holds. The nonlinear controller is first activated to swinging up the pendulum rod towards a small region around the upright position (unstable equilibrium), and the LQR controller is then activated to keep the IPS rod in vertical position. Each of these controllers is detailed below.
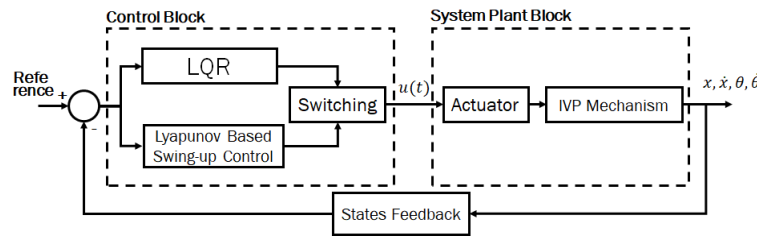
Figure 6. Block diagram of the switching controller

3.1. Nonlinear swing up control design

The construction of the nonlinear swinging up controller is done based on the analysis of the total energy that is required to swing the pendulum rod to reach a small region around the upright position that defines an unstable equilibrium. To this end, the IPS' total energy is first identified and defined (11).

$$E(q, \dot{q}) = E_K(q, \dot{q}) + E_P(q) = \frac{1}{2}\dot{q}^T M(q)\dot{q} + lmg(\cos\theta - 1) \tag{11}$$

the derivative of the system's energy in (11) with respect to time is given (12).

$$\dot{E}(q, \dot{q}) = \dot{q}^T M(q)\ddot{q} + \frac{1}{2}\dot{q}^T \dot{M}(q)\dot{q} + \dot{q}^T G(q) = \frac{1}{2}\dot{q}^T(\dot{M}(q) - 2C(q, \dot{q}))\dot{q} + \dot{q}^T F_M - \dot{q}^T D\dot{q}. \tag{12}$$

now notice the equilibrium of the state variable $\dot{x}$ when $E(q, \dot{q}) = 0$ for which condition (13) holds.

$$\frac{1}{2}l^2 m\dot{\theta}^2 = lmg(1 - \cos\theta) \tag{13}$$

As discussed in [14], $\dot{\theta} = 0\ rad$ implies (13) defines a homoclinic orbit. This means that $\theta := 0\ rad$ can only be achieved if $\dot{\theta} = 0\ rad$. Consequently, the pendulum rod will be swinging with reference to the vertical axis until arriving at the neighborhood of the equilibrium $[\theta, \dot{\theta}]^T = [0, 0]^T$. In the discussion that will follow, the following symmetric matrix term from the system model in (6) will also be useful.

$$\dot{M}(q) - 2C(q, \dot{q}) = \begin{bmatrix} 0 & lm\sin\theta \\ -lm\sin\theta & 0 \end{bmatrix} \tag{14}$$

Define $E(t) = E(q, \dot{q})$. Using (13) and (14), then (12) can be rewritten as: $\dot{E}(t) = \dot{q}^T F_M - \dot{q}^T D(\dot{q})\dot{q}$. Next, consider a quadratic candidate lyapunov function $V(t) := V(q, \dot{q})$ as (15).

$$V(t) = \frac{1}{2}\left(K_1 E^2 + K_2 \dot{q_1}^2 + K_3 q_1^2\right) \tag{15}$$

where $K_i,\ (i = 1, 2, 3)$ are positive constants. The time derivative of (15) can be computed as 16.

$$\dot{V}(t) = K_1 \dot{E}E + K_2 \ddot{q_1}\dot{q_1} + K_3 q_1 \dot{q_1} = K_1 E\left(u\dot{x} - \gamma_r\dot{\theta}^2\right) + K_2 \ddot{x}\dot{x} + K_3 \dot{x}x,$$
$$= \dot{x}\left(K_1 uE + K_2\ddot{x} + K_3 x\right) - K_1\gamma_r E\dot{\theta}^2 \tag{16}$$

notice that the term $\ddot{x}(t)$ in (16) can be obtained from (4) and is given by $\ddot{x}(t) = (\alpha + F_M)/\beta$ due to the impact that the friction force has on the system's disturbance with $\alpha = bm^2 l^2 x_4^2 + (M + m)(mgl\sin(x_3) - \gamma_r x_4)$ and $\beta = ml^2(M + m\sin^2(x_3))$. Using such a $\ddot{x}$ and control input $F_M = u(t)$, (16) can be written as (17).

$$\dot{V}(t) = \dot{x}\left(K_1 u(t)E + K_2(\alpha + u(t))\right)/\beta + K_3 x\right) - K_1\gamma_r E\dot{\theta}^2 \tag{17}$$

It can be seen that the second term $-K_1\gamma_r E(t)\dot{\theta}(t)^2$ on the right hand side (rhs) of (17) is always negative definite. This thus suggests that one needs to design a control law that can render the first term on the rhs of (7) to be negative definite [21]. In this regard, we consider a choice of control law as (18)

$$u(t) = \frac{-\beta(K_4\dot{x} + K_3 x) - K_2\alpha}{K_1\beta E + K_2} \tag{18}$$

where $K_4 > 0$ is a design parameter, and (i) $(K_1E + (K_2/\beta)) \neq 0$ and (ii) $(K_2/K_1) \neq -E(M + m \sin^2 \theta)$ are assumed on (18) to avoid singularity. Using the control signal in (18), then (17) can be expressed as (19).

$$\begin{aligned}
\dot{V}(t) &= u(t)\left(K_1E + K_2/\beta\right)\dot{x} + \left(K_2\alpha/\beta + K_3x\right)\dot{x} - K_1\gamma_r E\dot{\theta}^2 \\
&= \left(\frac{-\beta(K_4\dot{x} + K_3x) - K_2\alpha}{K_1\beta E + K_2}\right)\left(\frac{K_1\beta E + K_2}{\beta}\right)\dot{x} + \left(K_2\frac{\alpha}{\beta} + K_3x\right)\dot{x} - K_1\gamma_r E\dot{\theta}^2 \\
&= -K_4\dot{x}^2 - K_1\gamma_r E\dot{\theta}^2 < 0
\end{aligned} \tag{19}$$

Clearly, (19) shows the control law (18) ensures the Lyapunov function (15) has negative time derivative and is thus strictly decreasing. By lyapunov stability theorem, the system is guaranteed to be asymptotically stable. Since (11) implies $E(t) \geq -2lmg$, a constraint of the form $(K_2/K_1) < (2lgmM \simeq 0.0686)$ is also used.

3.2. Linear stabilizing control design

Once the nonlinear controller swings the pendulum rod into the neighborhood the unstable equilibrium, an LQR controller is used to stabilize the IPS system. The LQR control used in this paper is one which minimizes a quadratic cost function J of the form: $J = \arg\min \int_0^\infty \left(x(s)^\mathsf{T}Qx(s) + u(s)^\mathsf{T}Ru(s)\right) ds$, in which Q and R, respectively, are the state and control input weighting matrices [11], [22], [23]. The resulting control law is a state feedback control signal with a structure: $u(t) := -K_{LQR}x(t) = -R^{-1}B^\mathsf{T}Px(t)$, in which matrix P solves the algebraic Riccati equation of the form: $PA^\mathsf{T} + A^\mathsf{T}P - PBR^{-1}B^\mathsf{T}P = -Q$.

The weighting matrices Q and R are determined using Bryson's rule [24] such that: (i) $Q_{(k,k)} = (q_k^2)_{max}^{-1}$, for $k = 1, \ldots, n$, in which $n = \dim(q)$, and (ii) $R = (u_{max}^2)^{-1}$ where u_{max} is the maximum control input to the system and $(q_k)_{max}$ is the maximum value of the system states. In this paper, the cart's maximum translation state is constrained to $0.1\,m$ and the pendulum rod's stabilizing angle of deviation is set to $0.05\,rad$. These set the elements of $Q \in \mathbb{R}^{4 \times 4}$ to be: $Q_{1,1} = Q_{3,3} = \frac{1}{0.1^2} = 100$, and $Q_{2,2} = Q_{4,4} = \frac{1}{0.05^2} = 400$. By constraining the maximum control input to be $10\,N$, a weighting matrix $R = 1/(10^2) = 0.01$ is used.

4. RESULTS AND ANALYSIS
4.1. Simulation results

Two simulations were conducted in MATLAB to verify the derived model and controller of the IPS. The first one is to validate model (8) using an initial condition of $[x\ \dot{x}\ \theta\ \dot{\theta}]^\mathsf{T} = [0\ 0\ \pi\ 0]^\mathsf{T}$ and the following model parameters: $m = 0.05\,kg$, $M = 0.479\,kg$, $l = 0.143\,m$, $g = 9.81\,m/s^2$, $\gamma_r = 0.00016872\,Ns/rad$. A sampling time of $T_s = 5\,ms$ is used. Figure 7 plots the results of the first simulation for a constant input of $F_M = 1\,N$ in which the cart position is shown in Figure 7(a) while the rod angle response is shown in Figure 7(b). These plots show that the cart position keep increases while the pendulum rod oscillates until finally settles at the equilibrium $\theta = 3.34\,rad$. These results indicate that the used model is valid for a constant F_M.
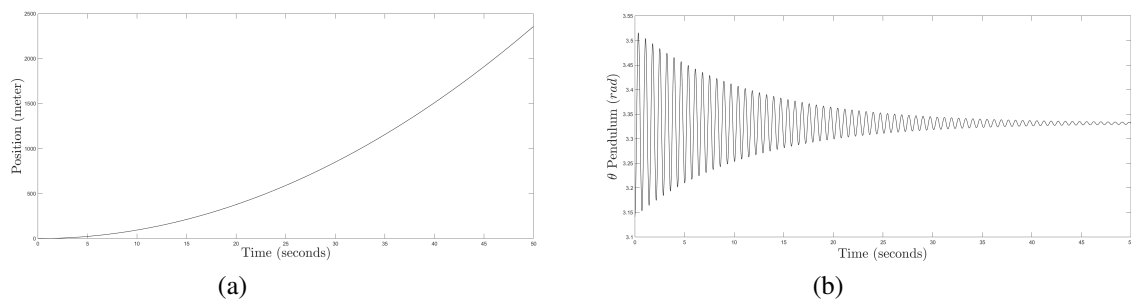

(a)

(b)

Figure 7. First simulation results for $F_M = 1N$: (a) cart position x and (b) rod angle θ

The second simulation was intended to check if the constructed nonlinear controller can swing the pendulum rod up towards a small region around the upright position (i.e., region of unstable equilibrium). The switching controller in Figure 6 was implemented to ensure the IPS is asymptotically stable. A similar set of model parameters was used while an initial condition with state values $[x\ \dot{x}\ \theta\ \dot{\theta}]^\mathsf{T} = [0.1\ 0\ \pi\ 0]^\mathsf{T}$ are used. The

gains of the nonlinear controller were chosen to be $[K_1\,K_2\,K_3\,K_4]^{\intercal} = [15\ 1\ 100\ 1]^{\intercal}$, and the LQR control gain was set to K_{LQR}=[-31.622 -222.081 -85.518 -66.643]$^{\intercal}$. Figure 8 plots the second simulation results. The controlled cart position in Figure 8(a) shows that it is shifting to $x = 0\ m$ when started at $x = 0.1m$. Consequently, the rod angle response in Figure 8(b) shows that it is eventually swinging up towards a small region around the vertical upright position of the equilibrium point $\theta = 0\ rad$ region. These plots thus demonstrate the proposed switching controller's effectiveness to stabilize the IPS platform model.
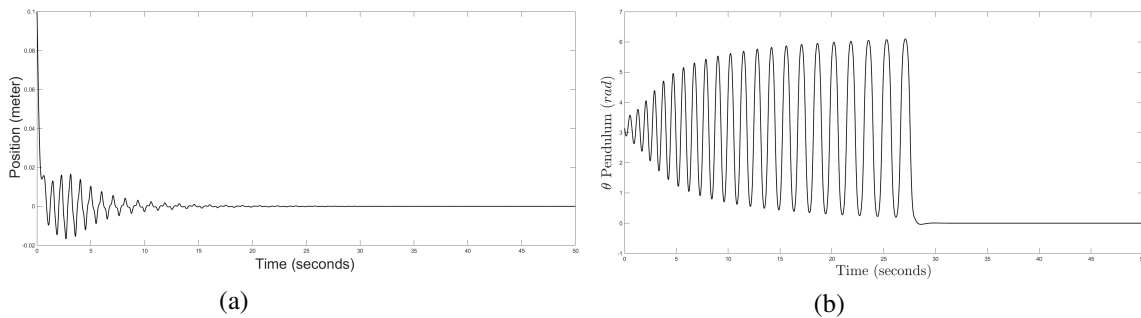

| (a) | (b) |

Figure 8. Second simulation results: (a) closed loop cart position x and (b) closed loop rod angle θ

4.2. Experimental results

The experimental validation of the switching controller was implemented on an Arduino microcontroller board to allow for the data transfer between PC controller and the IPS prototype. The used model parameters are similar with those used in simulations. The gain parameters of the nonlinear controller were set to be $[K_1,\,K_2,\,K_3,\,K_4]^{\intercal} = [29,\ 1,\ 100,\ 10]^{\intercal}$, while the gain parameters of the LQR controller were set to be K_{LQR}=[-63.24, -94.13, -382.24, -77.76]$^{\intercal}$. The initial conditions were set to: $[x,\,\dot{x},\,\theta,\,\dot{\theta}]^{\intercal}$=[0, 0, π, 0]$^{\intercal}$.

Figure 9 plots the experimental results of the proposed switching controller. The pendulum rod angle response shown in Figure 9(a) shows that the nonlinear controller part of the proposed switching controller brings the pendulum rod towards the neighborhood of the unstable equilibrium state ($\theta(t) = 0$), while the LQR controller stabilizes the rod at such an equilibrium point. The switching between the two controllers occurs at time $t = 14s$. Figure 9(b) which plots the phase portrait of the closed loop system experiment further shows that the angle trajectory starts at a homoclinic orbit to then finally stabilized at the equilibrium point of $\theta = 0^0$. The results depicted in these figures thus show the proposed switching controller's effectiveness to stabilize the IPS platform. A video demonstration of the switching controller implementation is available in [25].
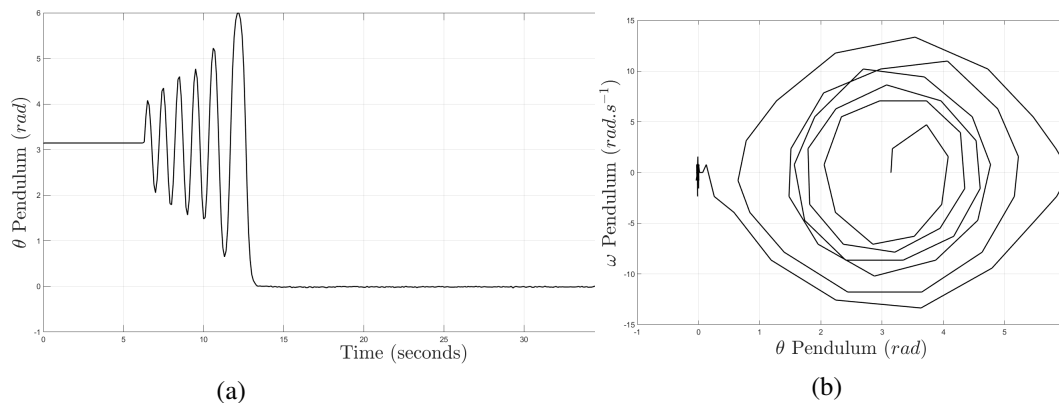

| (a) | (b) |

Figure 9. Results of experimental control implementation: (a) rod angle response and (b) phase portrait

5. CONCLUSION

This paper has presented an experimental implementation of a switching control scheme for an IPS platform on a cart. Such an implementation is demonstrated on the IPS dynamic model that is derived by Euler-Lagrange modeling formalism. The developed switching controller consists of a nonlinear lyapunov-based swing up controller which brings the pendulum rod towards a small region near the vertical upright position and an LQR controller which maintains the pendulum rod stable at the vertical axis. The results of both simulation and experimental implementations of the proposed switching controller are shown to demonstrate the effectiveness of the developed switching controller to stabilize the IPS at the desired equilibrium point.

REFERENCES

[1]   O. Boubaker, "The inverted pendulum benchmark in nonlinear control theory: a survey," *International Journal of Advanced Robotic Systems*, vol. 10, no. 5, p. 233, 2013, doi: 10.5772/55058.
[2]   M. F. Hamza, H. J. Yap, I. A. Choudhury, A. I. Isa, A. Y. Zimit, and T. Kumbasar, "Current development on using rotary inverted pendulum as a benchmark for testing linear and nonlinear control algorithms," *Mechanical Systems and Signal Processing*, vol. 116, pp. 347-369, 2019, doi: 10.1016/j.ymssp.2018.06.054.
[3]   D. Galan, D. Chaos, L. De La Torre, E. Aranda-Escolastico, and R. Heradio, "Customized online laboratory experiments: a general tool and its application to the furuta inverted pendulum," in *IEEE Control Systems Magazine*, vol. 39, no. 5, pp. 75-87, 2019, doi: 10.1109/MCS.2019.2925256.
[4]   E. Kennedy, E. King, and H. Tran, "Real-time implementation and analysis of a modified energy based controller for the swing-up of an inverted pendulum on a cart," *European Journal of Control*, vol. 50, no. 1, pp. 176-87, 2019, doi: 10.1016/j.ejcon.2019.05.002.
[5]   G. Rigatos, K. Busawon, J. Pomares, and M. Abbaszadeh, "Nonlinear optimal control for the wheeled inverted pendulum system," *Robotica*, vol. 38, no. 1, pp. 29-47, 2020, doi: 10.1017/S0263574719000456.
[6]   S. Maity and G. R. Luecke, "Stabilization and optimization of design parameters for control of inverted pendulum," *Journal of Dynamic Systems, Measurement, and Control*, vol. 141, no. 8, p. 081007, 2019, doi: 10.1115/1.4042953.
[7]   F. Rubio, F. Valero, and C. Llopis-Albert, "A review of mobile robots: Concepts, methods, theoretical framework, and applications," *International Journal of Advanced Robotic Systems*, vol. 16, no. 2, p. 1729881419839596, 2019, doi: 10.1177/1729881419839596.
[8]   A. Delgado-Spíndola, R. Campa, E. Bugarin, and I. Soto, "Design and real-time implementation of a nonlinear regulation controller for the RMP-100 Segway TWIP," *Mechatronics*, vol. 79, no. 1, p. 102668, 2021, doi: 10.1016/j.mechatronics.2021.102668.
[9]   A. M. A. Shalaby, "Evaluation of the performance of a rocket under oscillatory thrust," M.S. thesis, Dept. Mechanical and Aerospace Eng., California State University, 2019.
[10]   M. Massaro, S. Lovato, and D. J. Limebeer, "The optimal erection of the inverted pendulum," *Applied Sciences*, vol. 12, no. 16, p. 8112, 2022, doi: 10.3390/app12168112.
[11]   T. Johnson, S. Zhou, W. Cheah, W. Mansell, R. Young, and S. Watson, "Implementation of a perceptual controller for an inverted pendulum robot," *Journal of Intelligent and Robotic Systems*, vol. 99, pp. 683-692, 2020, doi: 10.1007/s10846-020-01158-4.
[12]   T. Yamakawa, "Stabilization of an inverted pendulum by a high-speed fuzzy logic controller hardware system," *Fuzzy Sets Systems*, vol. 32, no. 2, pp. 161-180, 1989, doi: 10.1016/0165-0114(89)90252-2.
[13]   E. Susanto, A. S. Wibowo, and E. G. Rachman, "Fuzzy swing up control and optimal state feedback stabilization for self-erecting inverted pendulum," *IEEE Access*, vol. 8, no. 1, pp. 6496-504, 2020, doi: 10.1109/ACCESS.2019.2963399.
[14]   M. J. Blondin and P. M. Pardalos, "A holistic optimization approach for inverted cart-pendulum control tuning," *Soft Computing*, vol. 24, no. 6, pp. 4343-4359, 2020, doi: 10.1007/s00500-019-04198-7.
[15]   R. Lozano, I. Fantoni, and D. J. Block, "Stabilization of the inverted pendulum around its homoclinic orbit," *Systems and Control Letters*, vol. 40, no. 3, pp. 197-204, 2000, doi: 10.1016/S0167-6911(00)00025-6.
[16]   T. Maeba, M. Deng, A. Yanou, and T. Henmi, "Swing-up controller design for inverted pendulum by using energy control method based on Lyapunov function," *Proceedings of the 2010 International Conference on Modelling, Identification and Control*, 2010, pp. 768-773.
[17]   A. Siuka and M. Schöberl, "Applications of energy based control methods for the inverted pendulum on a cart," *Robotics and Autonomous Systems*, vol. 57, no. 10, pp. 1012-1017, 2009, doi: 10.1016/j.robot.2009.07.016.
[18]   J. Chandra, T. A. Tamba, and A. Sadiyoko, "Energy-based modeling and swing up control synthesis of an inverted pendulum system," *2019 International Conference on Mechatronics, Robotics, and Systems Engineering*, pp. 265-269, 2019, doi: 10.1109/MoRSE48060.2019.8998729.
[19]   C. A. Ibanez, O. G. Frias, and M. S. Castanon, "Lyapunov-based controller for the inverted pendulum cart system," *Nonlinear Dynamics*, vol. 40, no. 4, pp. 367-374, 2005, doi: 10.1007/s11071-005-7290-y.
[20]   A. Tiga, C. Ghorbel, and N. Benhadj Braiek, "Nonlinear/linear switched control of inverted pendulum system: stability analysis and real-time implementation," *Mathematical Problems in Engineering*, vol. 2019, pp. 1-10, 2019, doi: 10.1155/2019/2391587.
[21]   P. Zhou, X. Hu, Z. Zhu, and J. Ma, "What is the most suitable Lyapunov function?," *Chaos Solitons Fractals*, vol. 150, no. 9, p. 111154, 2021, doi: 10.1016/j.chaos.2021.111154.

[22] J. P. Hespanha, *Linear Systems Theory*, 2nd ed. Princeton, NJ: Princeton University Press, 2018. [Online]. Available: https://press.princeton.edu/books/ebook/9781400890088/linear-systems-theory.

[23] S. Trimpe, A. Millane, S. Doessegger, and R. D'Andrea, "A self-tuning LQR approach demonstrated on an inverted pendulum," *IFAC Proceedings Volumes*, vol. 47, no. 3, pp. 11281-11287, 2014, doi: 10.3182/20140824-6-ZA-1003.01455.

[24] T. M. Tijani, and I. A. Jimoh, "Optimal control of the double inverted pendulum on a cart: A comparative study of explicit MPC and LQR," *Applications of Modelling and Simulation*, vol. 5, pp. 74-87, 2021.

[25] J. Chandra, T.A. Tamba, and A. Sadiyoko, *Switching Control of an Inverted Pendulum Systems.* (2023). Accessed: Dec. 23, 2023. [Streaming Video]. Available: https://drive.google.com/file/d/14-ttgsKM6qVlzNarrygcPi5T3GHHLZIp/view?usp=sharing.

BIOGRAPHIES OF AUTHORS

Jonathan Chandra received a B.Eng degree in Electrical Engineering from Parahyangan Catholic University in 2020, and a M.Sc degree in Mechanical Engineering from University of Groningen in 2023. He is currently pursuing his Ph.D degree in Mechanical Engineering at University of Groningen, The Netherlands. His research interests include control systems design for mechatronics and robotic systems. He can be contacted at email: J.chandra.1@student.rug.nl.

Tua Agustinus Tamba is an assistant professor in the Department of Electrical Engineering at Parahyangan Catholic University, Indonesia. He received his MSEE and Ph.D in Electrical Engineering from University of Notre Dame (USA) in 2016, M.Sc in Mechanical Engineering from Pusan National University (Republic of Korea) in 2009, and B.Eng in Engineering Physics from Institut Teknologi Bandung (Indonesia) in 2006. His research interests include dynamical systems, control theory, and optimization with applications in mechatronics, robotics, automation systems, and systems biology. He can be contacted at email: ttamba@unpar.ac.id.

Ali Sadiyoko is presently an associate professor in the Department of Electrical Engineering at Parahyangan Catholic University. He received both his B.Eng and Doctoral degree in Electrical Engineering from Institut Teknologi Bandung (Indonesia) in 1995 and 2016, respectively. His has worked on researh projects related to the modeling and control of multi-agent system dynamics and collaborative robots. He can be contacted at email: alfa51@unpar.ac.id.